

Team 5 Final Report – Project A – Supersonic Inlet

Michael Ogawa, Erik Buth, and Saron Bhoopathy

Abstract

The Fluent solver was used to study the flow through the NASA 1507 which is a Mach 3, axisymmetric-spike, mixed compression inlet. The objective was to compare simulation results to different solver processes and to wind-tunnel data. The 2D geometry was meshed to create unstructured grids of 42,885 and 92,753 nodes with inflation layers near the walls. Simulations were run using the Second Order Upwind method for the flow and the turbulent dissipation rates, and the QUICK method for the turbulent kinetic energy. Three simulations were performed by varying the backpressure at the engine face and in the bleed regions. An internal shock structure was observed with oblique shocks of increasing turn angle. The shock pattern ends with a terminal normal shock downstream of the throat producing subsonic flow at the engine face with minimal total pressure loss. Increasing the backpressure resulted in the terminal shock moving closer to the throat. Shock-boundary layer interactions and bleed zone effects on the boundary layer thickness were resolved in both grids. Another simulation was performed at the off-design condition of Mach 2 to study the behavior of the inlet. This led to the formation of a detached bow shock at the inlet face which resulted in significant total pressure loss at the engine face. The simulation results showed strong correlation to the simulation results published by PAW-6 and to wind-tunnel data with comparable internal shock pattern, terminal shock location, and outlet total pressure values.

Introduction

This assignment was based on the project for the 6th AIAA Propulsion Aerodynamics Workshop (PAW-6), whose goal is to assess the accuracy of existing CFD codes in simulating propulsion-related flows. Specifically, this project aimed simulate a mixed-compression inlet with an internal shock structure and porous bleed regions. The inlet, shown in fig. 1, is what is referred to as the NASA 1507 inlet, which is a Mach 3, axisymmetric-spike, mixed-compression inlet which was developed and tested at NASA Ames in the late 1960s. The geometry and test results were reported by Sorensen and Smeltzer in the NASA TM X-1507 report [1]. The inlet was selected due to its geometric simplicity, public availability, and published wind-tunnel data.

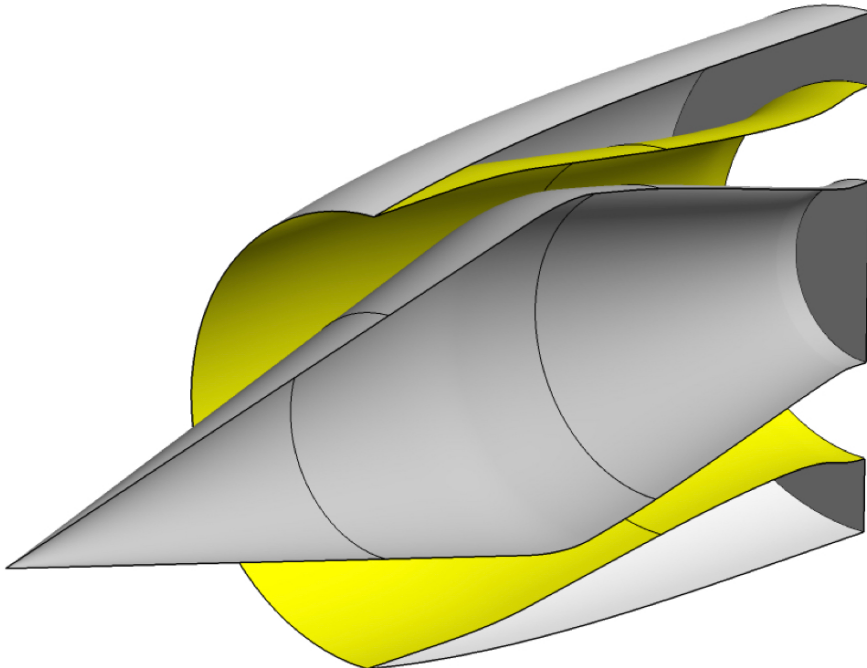


Figure 1: NASA 1507 inlet geometry [1]

The 2D axisymmetric geometry is labelled and highlighted in fig. 2 along with the flow domain. The inlet consists of a center-body spike that acts as a converging-diverging nozzle. A

cowl is present to establish the internal shock structure. A total of four bleed regions are present in both the cowl and center-body to energize the boundary layer and prevent flow separation due to shock-boundary layer interactions. The inlet was designed such that the internal shock structure slowly turned the flow before ending with a terminal shock. This ensures minimal total pressure losses and production of subsonic flow at the engine face. The inlet serves two purposes in a typical turbojet engine, first is to compress the incoming air and second to slow supersonic flow to subsonic speeds as required by the turbomachinery.

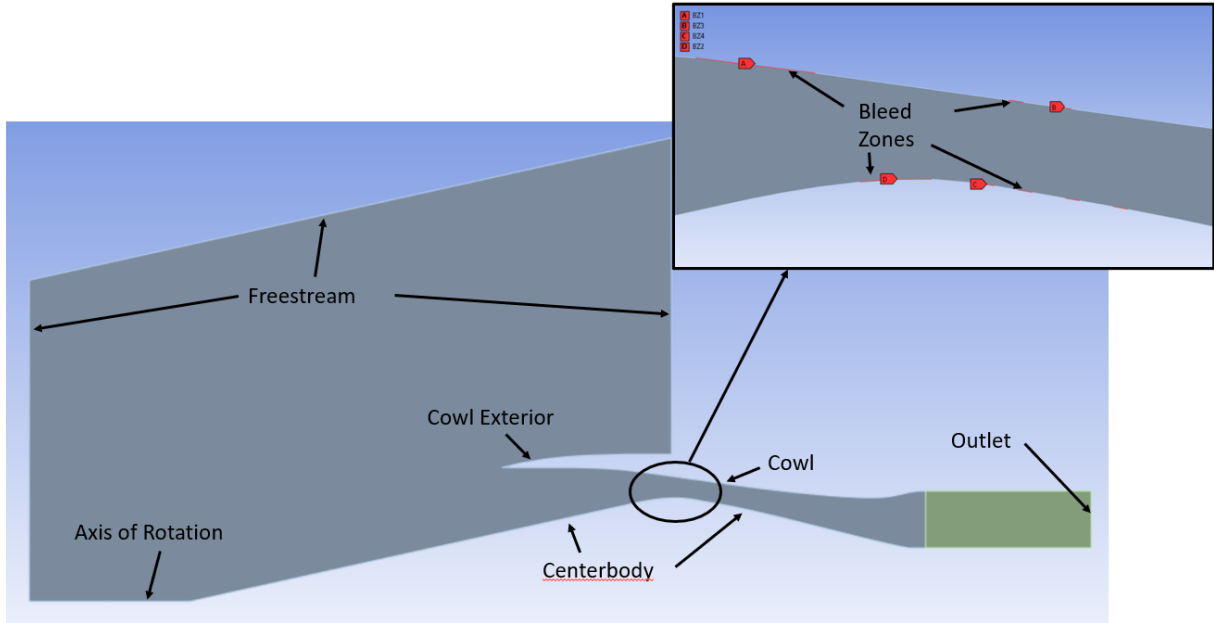


Figure 2: Geometry of the Problem

For all three test cases, the inlet conditions were kept the same. These are summarized in Table 1. For the extra test case, the freestream Mach number was changed from 3 to 2. The outlet and bleed zone boundary conditions were changed between each test case. Those are described in more detail in the Analysis section below.

Table 1: Inlet Condition Parameters

Parameter	Value	Unit
M_∞	3.0	
$p_{t,\infty}$	15.0	psi
p_∞	0.4084	psi
R_n	2.00E+06	/ft
T_∞	220.0	R
$T_{t,\infty}$	616.0	R
γ	1.4	
R	1716.245	ft-lbf slug-R
g_c	32.174	lbf slug
R_c	10.0	in
D_c	20.0	in
A_c	314.16	in^2
m_∞	0.7411	slug/sec

Numerical Solution

Two grids were generated and used for this problem, a coarse grid and a medium grid. Full views of each grid can be seen in fig. 3 and fig. 6, respectively. The coarse grid was an unstructured mesh with inflation layers near the wall in order to effectively capture the boundary layers and their interaction with the shocks. The inflation layers can be seen more clearly in figs. 4 and 5 for the coarse grid, and figs. 7 and 8 for the medium grid. To size the inflation layers, it was assumed that the walls along the entire length of the inlet were flat plates. This assumption seemed reasonable enough, as the purpose of the bleed zones was to prevent any boundary layer separation along the length of the inlet. Then, using the Blasius flat plate equations, a first layer cell size y_1 was determined by finding the location where $y^+ = 30$. A growth rate of 1.2 was set for the layers, and 15 layers were added. Using this method, the initial cell size around the inlet center-body was $1.35e-4$ m. The initial cell size around the inlet cowl was $1.28e-4$ m. The unstructured cell meshing for the rest of the region not impacted by the inflation layers was then adjusted to limit the aspect ratio of the cells to less than 1000, as recommended. Doing so, we

get a face sizing element size of 5e-3m for the mesh. This means that the entire mesh consists of 42,885 cells.

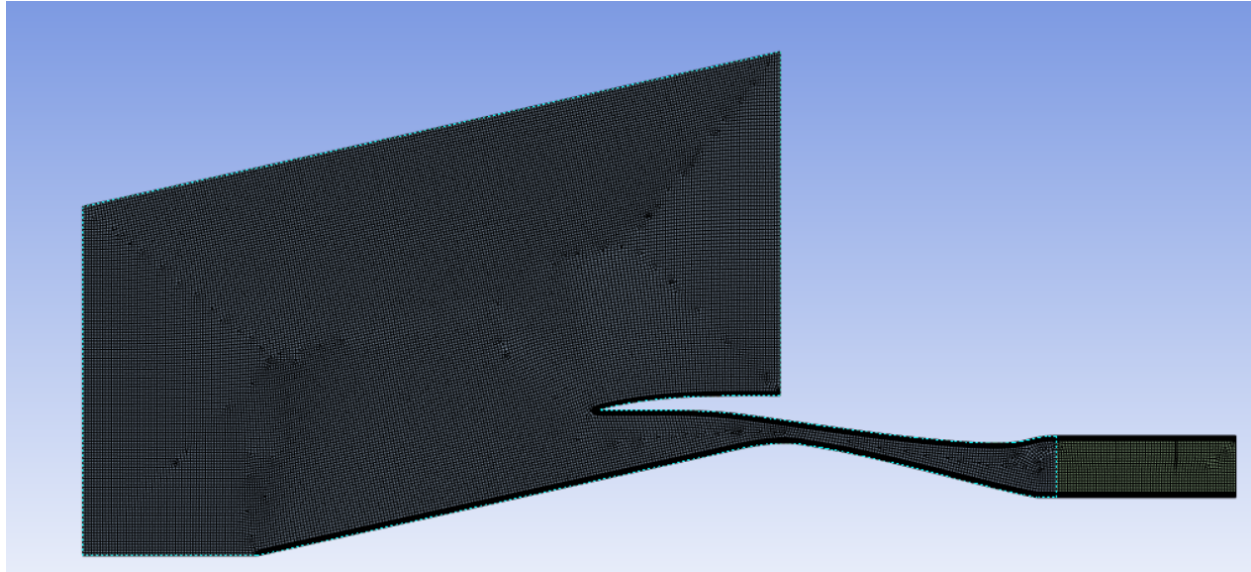


Figure 3: Full View of Coarse Grid

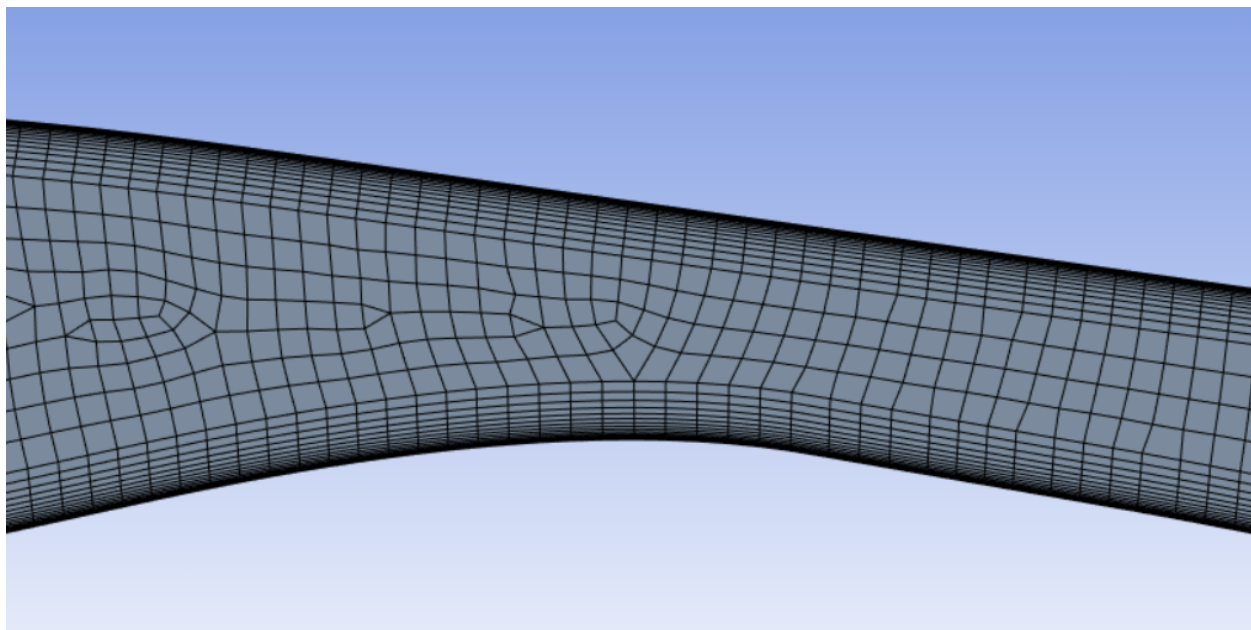


Figure 4: Throat Region of the Coarse Grid

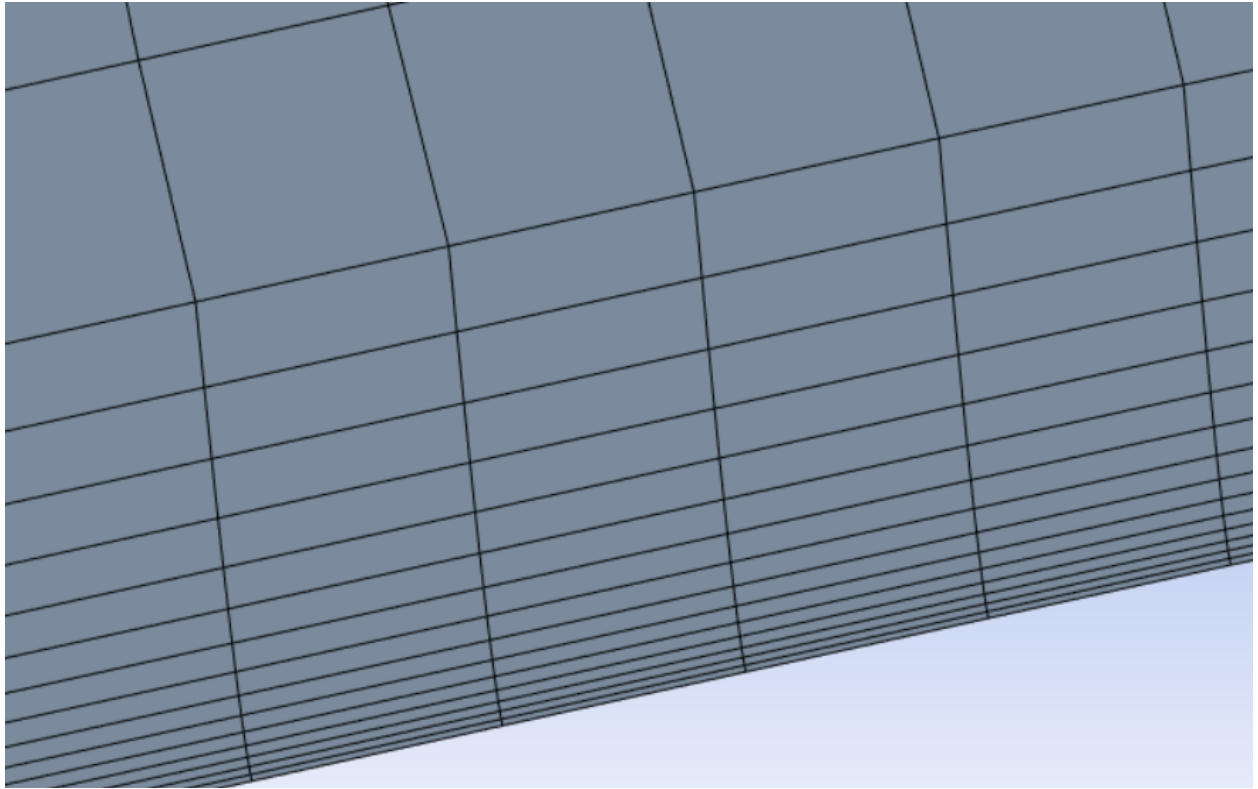


Figure 5: Inflation Layers Near Centerbody of the Coarse Grid

It was desired that the medium grid had at least double the number of cells compared to the coarse grid. In order to accomplish this, all cell size values were reduced by a factor of 1.5. This meant that the y_1 value for the center-body inflation layer changed to $9.570\text{e-}5\text{m}$. The y_1 value for the inlet cowl changed to $9.078\text{e-}5\text{m}$. The face sizing element size changed to $3.333\text{e-}5\text{m}$. In addition, the number of inflation layers was increased from 15 to 20. These changes created a grid with 92,753 grid points, more than double the number of grid points of the coarse grid.

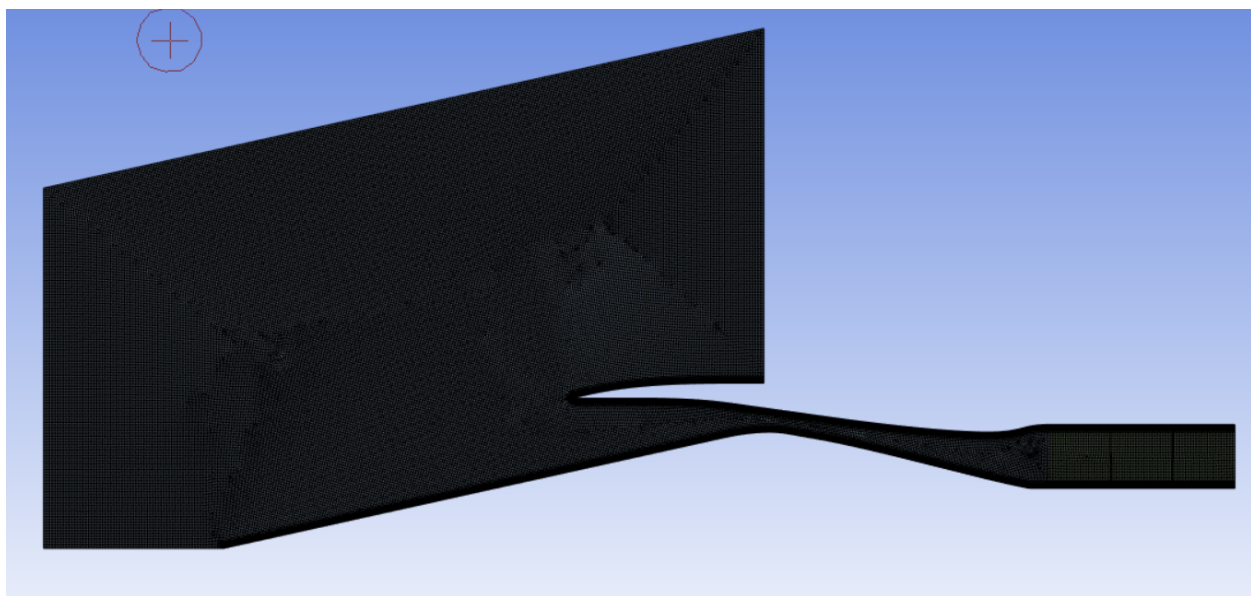


Figure 6: Full View of Medium Grid

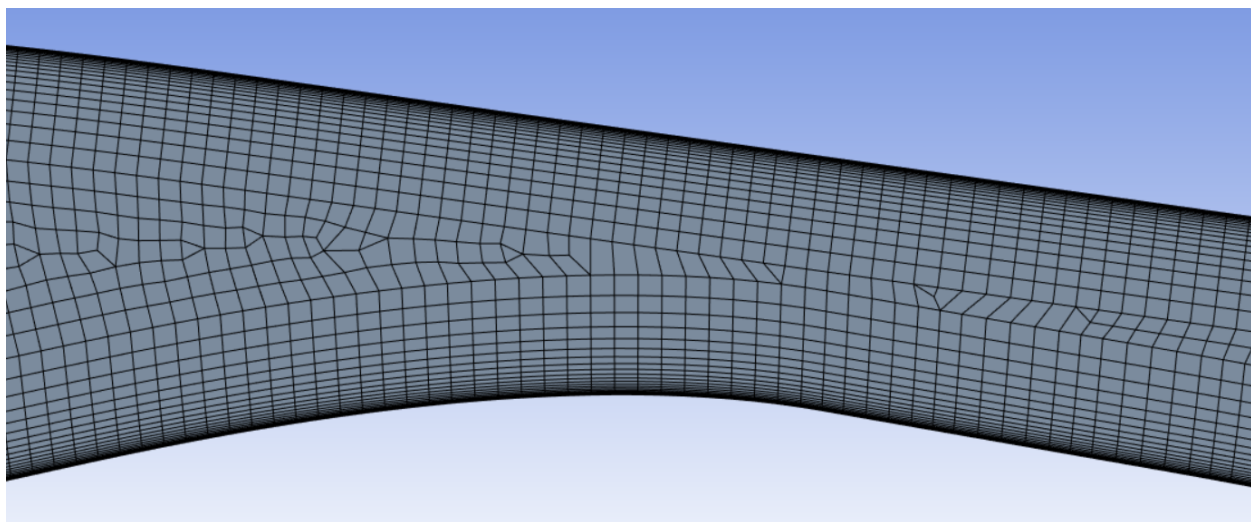


Figure 7: Throat Region of Medium Grid

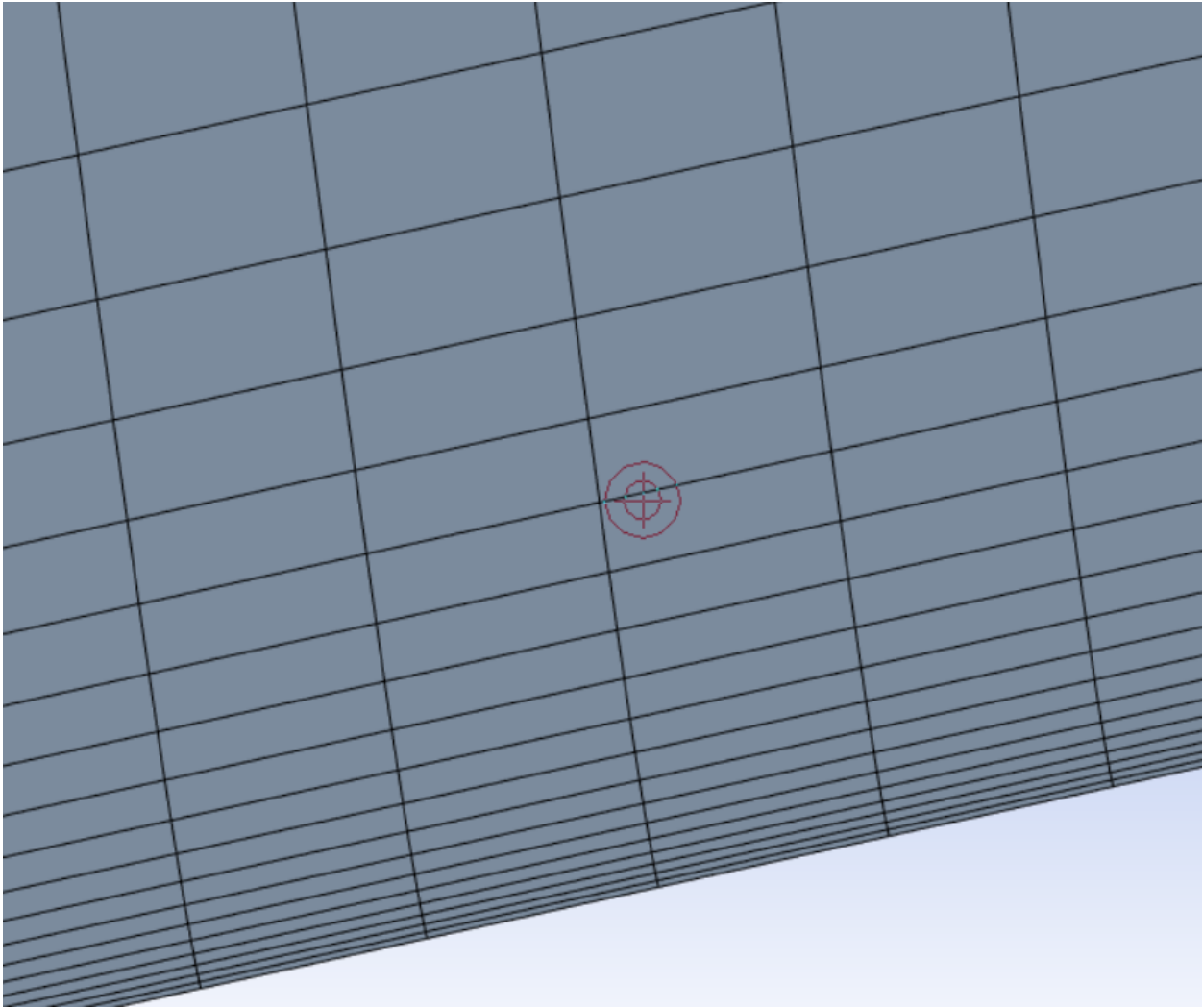


Figure 8: Inflation Layers Near Centerbody of Medium Grid

To run Fluent to find a solution, the AAE Computer Lab computers were used. Double precision was used in the setup, and either 4 or 6 cores were used, depending on the user. A density-based, axisymmetric solver was selected. The k-epsilon model for turbulence with simple wall functions was used, and thermal models were turned on. Air was selected as the material, with ideal gas assumptions used. The desired residuals for all flow characteristics were set at 0.001, the default value. All other settings were left as the default settings. In order to converge at a single solution, two stages were used. In the first stage, a First Order Upwind method was used to solve for the flow, turbulent kinetic energy, and the turbulent dissipation

rate. The Courant number was set at 1. The solution was then run until either the residuals converged, or the residuals oscillated for around 1000 iterations. For stage one, this took approximately 8000 iterations. In stage two, a Second Order Upwind method was used to solve for the flow and the turbulent dissipation rate, and the QUICK method was used to solve for the turbulent kinetic energy. The Courant number remained unchanged. This ensured that our final solution would be at least second order accurate, as required. This was run until the solution converged or started oscillating for around 1000 iterations. This took approximately 6000 additional iterations, for a total of around 14000 iterations in order to come to a final solution.

The boundary condition settings used are summarized in the fig. 9 below. For the pressure outlet boundary conditions used for the bleed zones and the outlet, the “prevent backflow” option was chosen. This boundary condition would convert any outlet to a solid wall boundary condition in the event backflow would otherwise occur, which helped keep the solution from diverging during the first few thousand iterations.

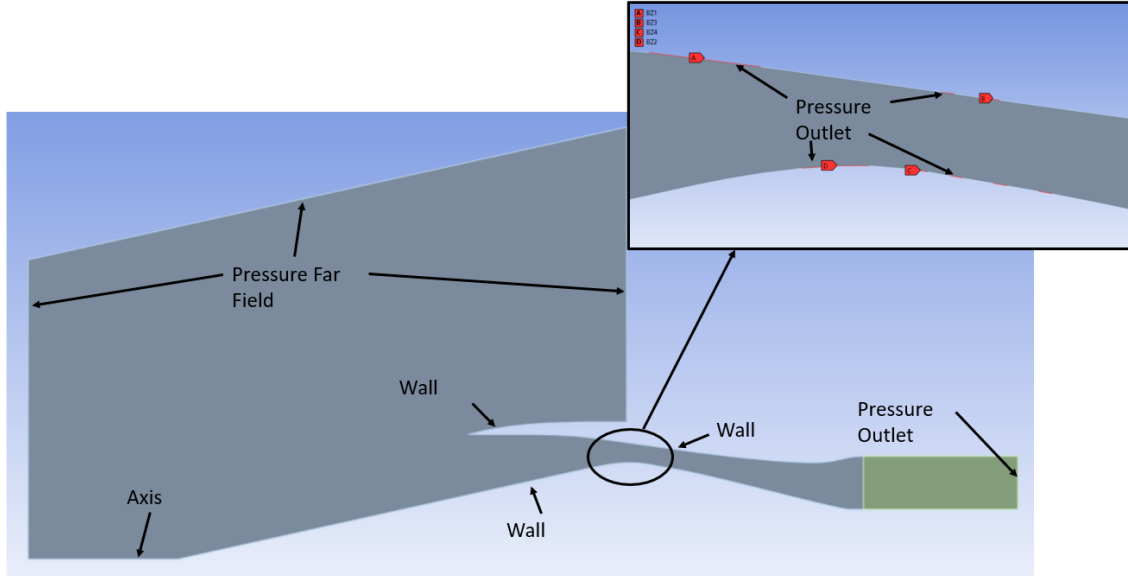


Figure 9: Boundary Condition Options Used

Results

The boundary conditions used for the three test cases in the bleed regions and at the engine face are highlighted in Table 1. The results for each of the three test cases, as well as the extra test case, can be seen in the figures below. Figs. 10, 13, and 16 are the coarse grid Mach contours of test cases 2, 4, and 8 respectively. The first, most noticeable result between the three main test cases is that increasing the backpressure of the inlet moves the location of the normal shock closer to the throat of the inlet. In Fig. 10, the normal shock is downstream of the bleed zones. In Fig. 13, with increased backpressure, the normal shock moves to be between the bleed zones but downstream of the throat. Test case 8, with the highest backpressure, was described as the engine operating conditions right before unstart occurred. This matches with the results in fig. 16 showing the normal shock nearly at the throat of the inlet. The extra case was simulated using test case 2 conditions at an off-design Mach number of 2. This results in the formation of a bow shock in front of the inlet as observed in fig. 19.

Table 2: Values of total pressure used in the bleed regions and engine face for three test cases

Test Case	P_{tbl1} (Pa)	p_{tbl2} (Pa)	p_{tbl3} (Pa)	p_{tbl4} (Pa)	p_{t2} (Pa)
2	12307	15513	10859	19443	84185
4	12617	15720	19650	27303	91528
8	12824	16444	31233	39507	94113

Figs. 11, 14, and 17 are the medium grid Mach contours of test cases 2, 4, and 8 respectively. These figures highlight the effect the bleed zones and oblique shocks on the boundary layers with higher resolution than in the coarse grids. In all three figures, it can be

clearly seen that whenever an oblique shock or the normal shock hits a wall, it increases the size of the boundary layer. This is the effect of the shock-boundary layer interaction. The bleed zones have the effect of decreasing the size of the boundary layer by energizing the boundary layer and delaying its growth caused by the shocks and the curved geometry of the inlet. The bleed zones are only effective in decreasing the size of the boundary layer only if they occur after the oblique shocks and before the normal shock. In test case 2, for example, it can be clearly seen that the boundary layer grows quickly in size along the engine cowl due to the normal shock occurring after all the bleed zones at the top.

The operating conditions for each test case gave us the desired outlet total pressures for the inlet. Figs. 12, 15, and 18 show the total pressure profile at the outlet for test cases 2, 4, and 8, respectively. It was observed that the total pressure distribution varied along the radial direction at the engine face as highlighted in the three figures. In all three cases, the total pressure was low near the inlet center-body and the cowl. The pressure then increased towards a peak somewhere in the middle of the flow domain. The exact shape and distribution were dependent on the test case, as well as the grid used, but the general trend held among all three cases. The exit pressure was determined to be “correct” when the target total pressure was around halfway between the minimum and maximum total pressure of the distribution.

Fig. 19 is the Mach contour of the off-design condition of Mach 2 run on the medium grid. The internal shock pattern is abolished and a detached or bow shock forms at the front face of the inlet. Majority of the supersonic velocity is lost after this shock and the flow reaches subsonic levels downstream of the throat. Therefore, the engine is still operable at the off-design condition. However, in fig. 20, the total pressure profile can be seen at the outlet to be around 71,300 Pa as opposed to the 84,185 Pa as observed in test case 2. Therefore, the presence of the

internal shock structure and the slow compression of the flow leads to minimal total pressure losses and increased engine efficiency. In the off-design case of Mach 2, significant total pressure losses occur leading to reduced engine efficiency.

Refining the grid from coarse to medium had a couple of notable effects. As previously mentioned, refining the grid had the effect of changing the total pressure distribution at the outlet. For test cases 2 and 8, the only effect it had was in increasing the peak total pressure. For test case 4, refining the grid lowered the peak total pressure, and moved the peak total pressure to be closer to the inlet cowl as opposed to the center-body. An additional effect was that the oblique shocks inside the inlet became more defined. This was especially prevalent at and just after the throat, where the distance between each shock was becoming shorter and shorter. Lastly, the results of test case 2 are compared with the simulations results published by PAW-6 [2] in fig. 21. As it can be seen, the internal shock structure and shock-boundary layer interactions are nearly identical between the two results. However, in the published results, the normal shock is slightly downstream of the normal shock in our results.

Because we assumed that the boundary layer was attached along the entire length of the inlet, we got a y_1 value for each wall which was larger than what we would have had if we did not make that assumption. This likely meant that, especially closer to the inlet and around the bleed zones, some details about the flow could have been lost. In fact, refining the grid from coarse to medium, where the inflation layers were also reduced in size, did result in some extra detail about the boundary layers being captured, notable along the engine center-body after the first oblique shock hits the boundary layer.

There are two major improvements which could be made to our grid which would help improve the quality of the solution. First off, to better capture the shape of the shocks, patching

could be used in regions with a high total pressure gradient in order to refine the grid. Second, the areas around the bleed zone include some rapid changes in flow direction and magnitude which is not accurately captured using our current grid. Refining the size of the grid near the bleed zones, whether by patching or some other method, would be better able to capture the characteristics of the flow near the bleed zones.

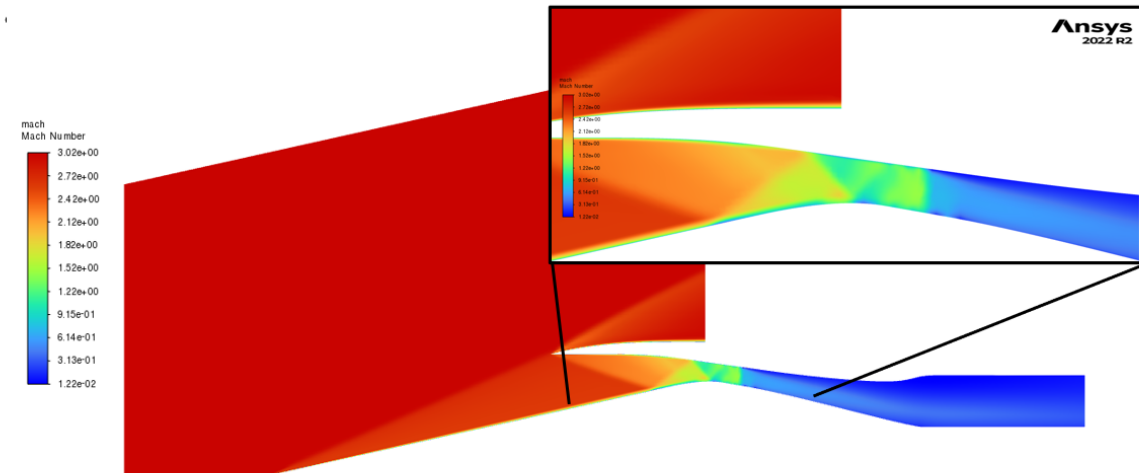


Figure 10: Test Case 2 Coarse Grid Mach Contour

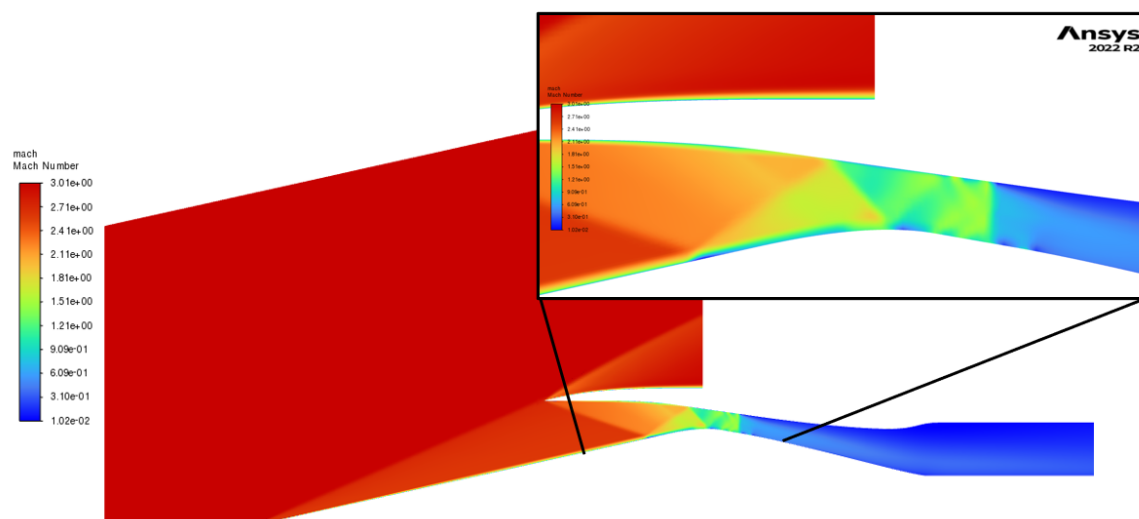


Figure 11: Test Case 2 Medium Grid Mach Contour

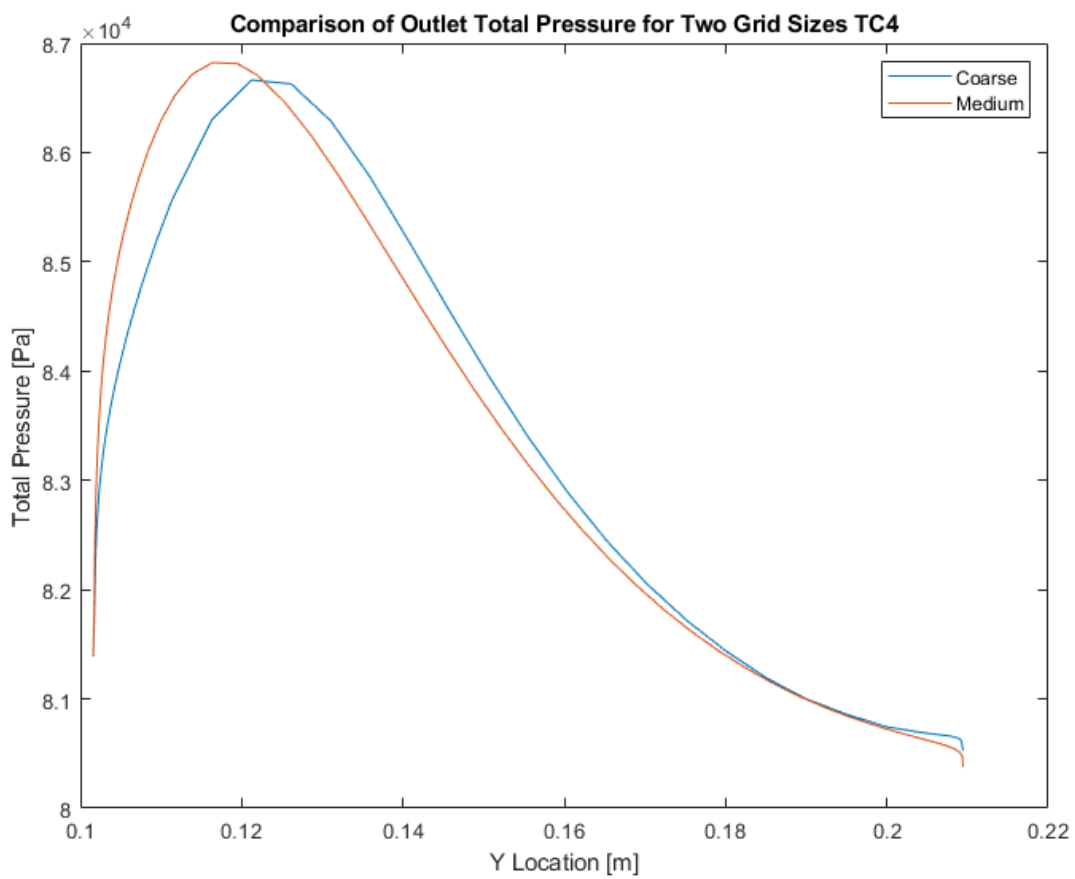


Figure 12: Test Case 2 Pressure Outlet

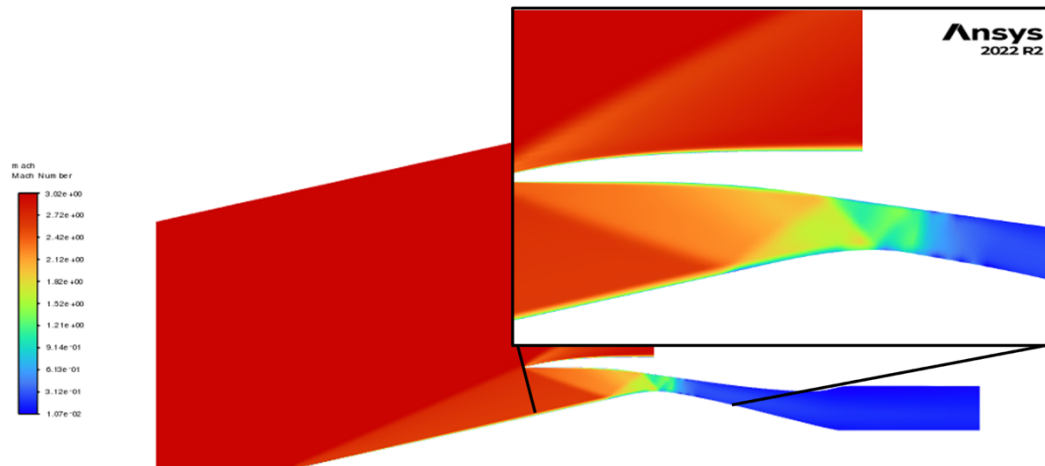


Figure 13: Test Case 4 Coarse Grid Mach Contour

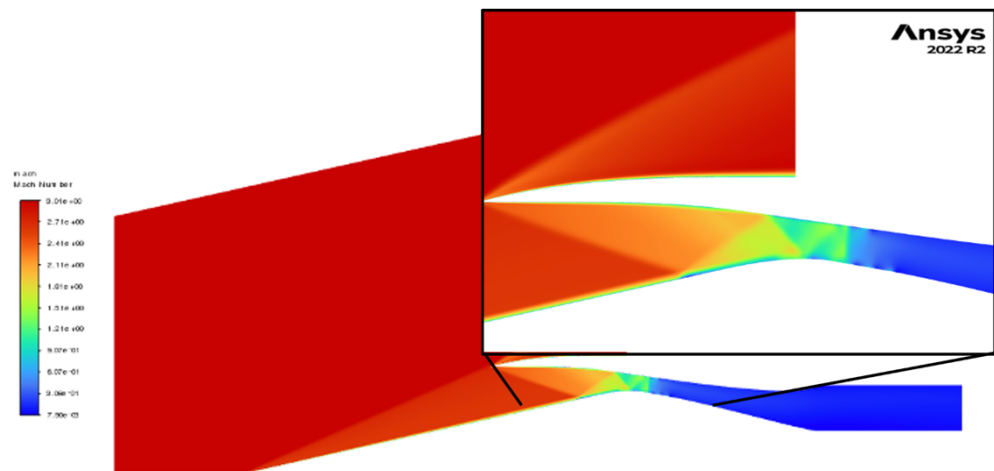


Figure 14: Test Case 4 Medium Grid Mach Contour

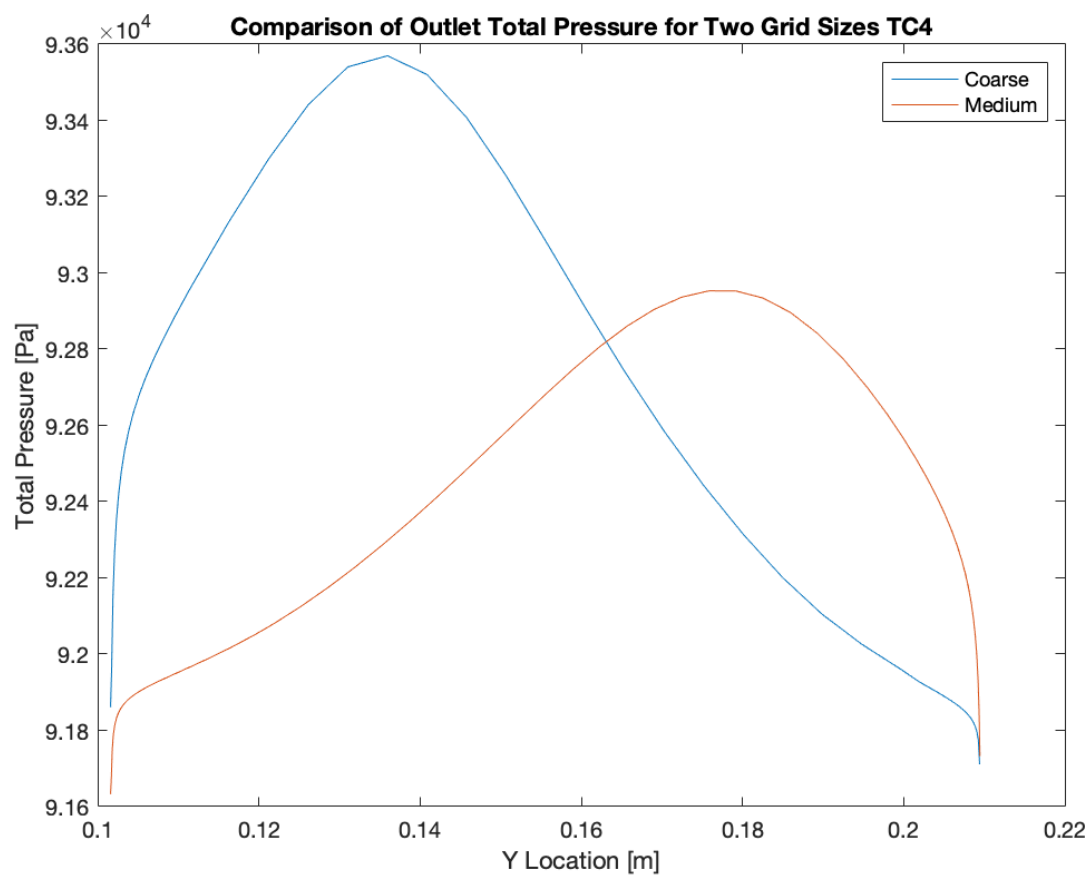


Figure 15: Test Case 4 Pressure Outlet

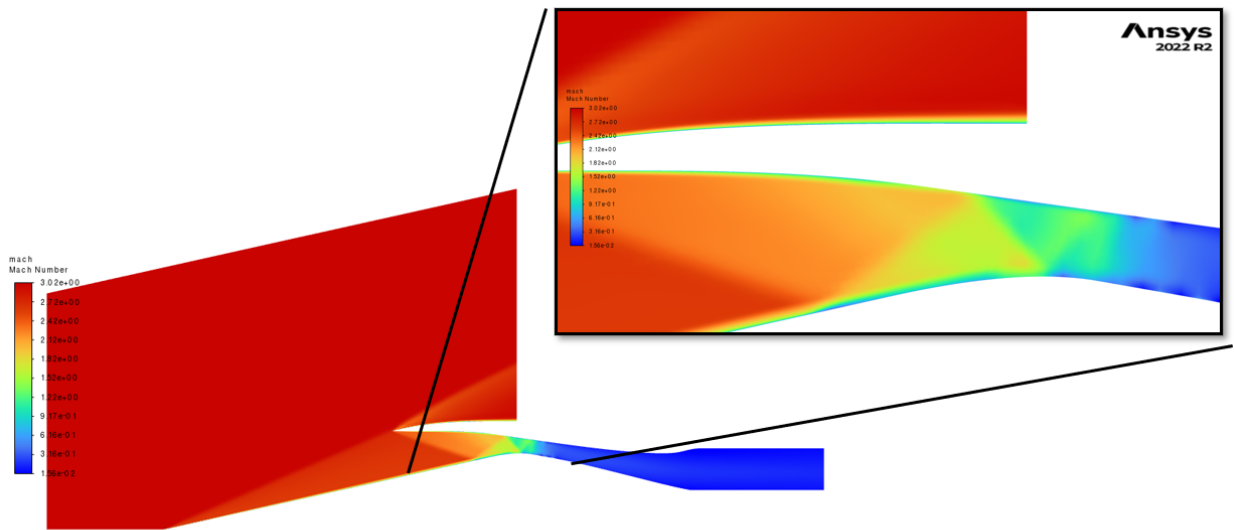


Figure 16: Test Case 8 Coarse Grid Mach Contour

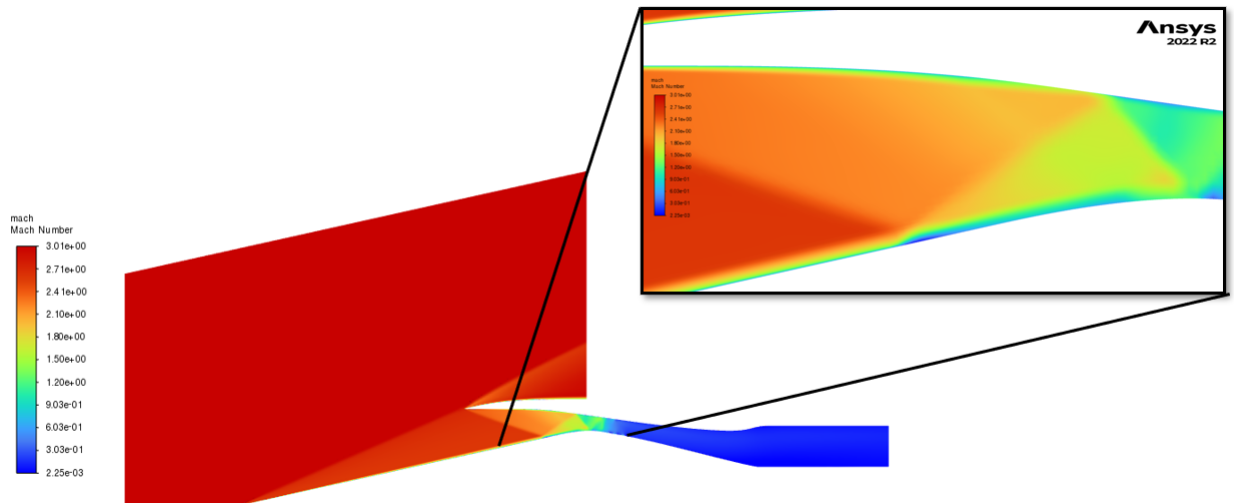


Figure 17: Test Case 8 Medium Grid Mach Contour

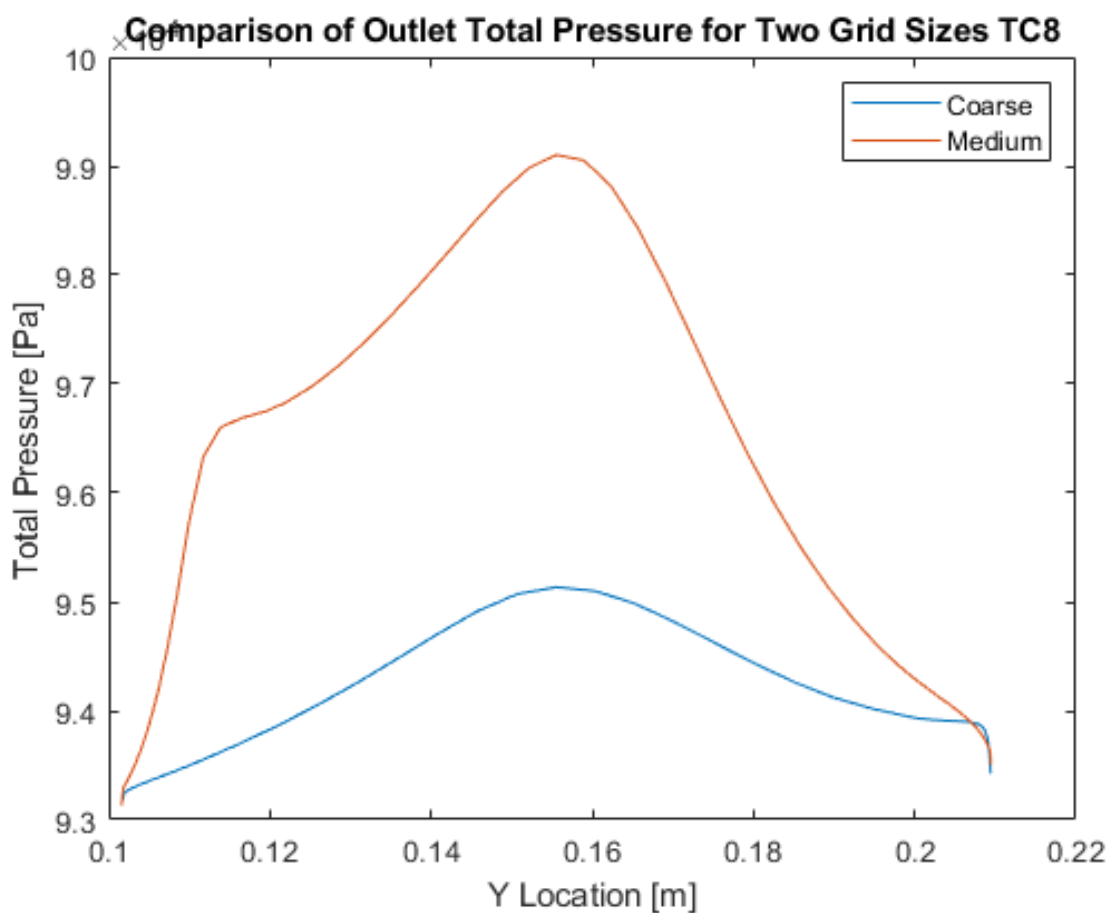


Figure 18: Test Case 8 Pressure Outlet

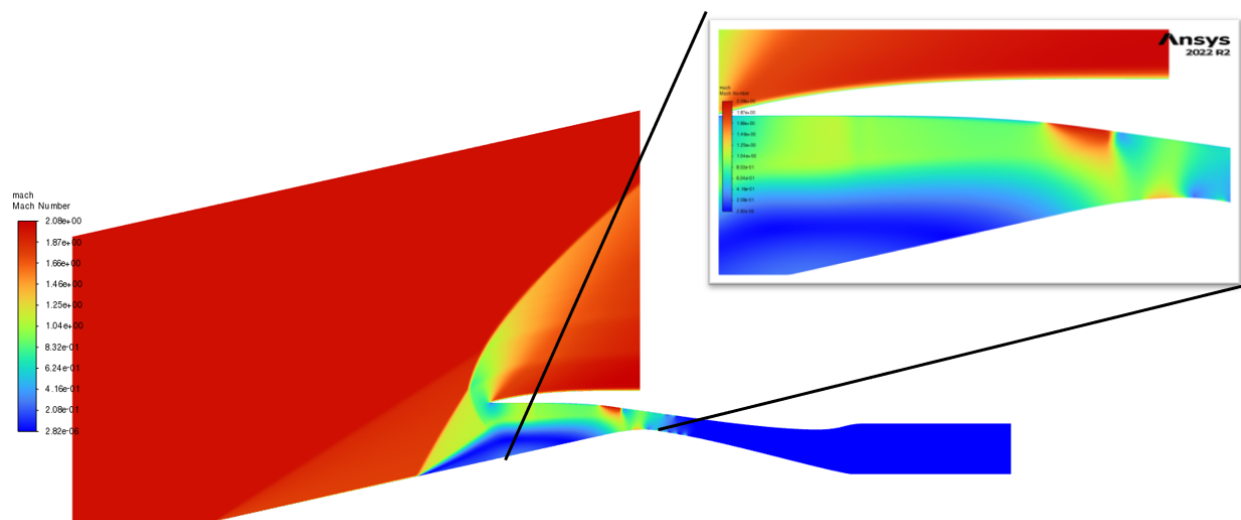


Figure 19: Extra Case, Test Case 2 with Mach = 2 Mach Contour (Medium Grid Only)

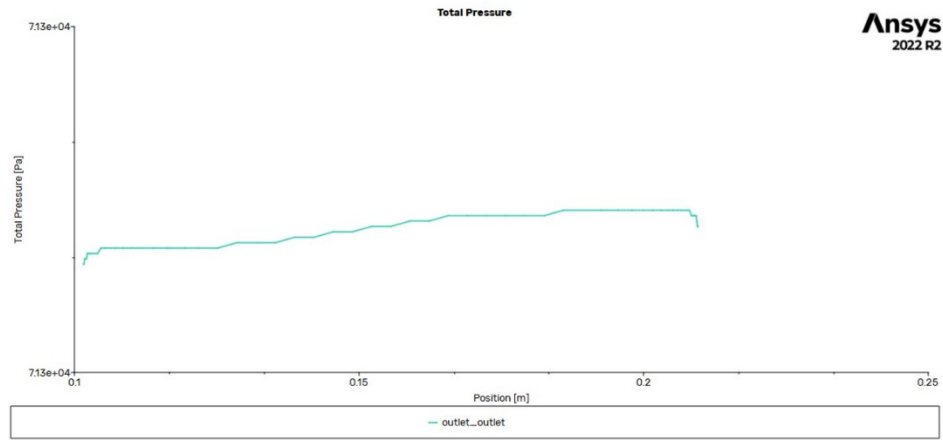


Figure 20: Extra Case Pressure Outlet

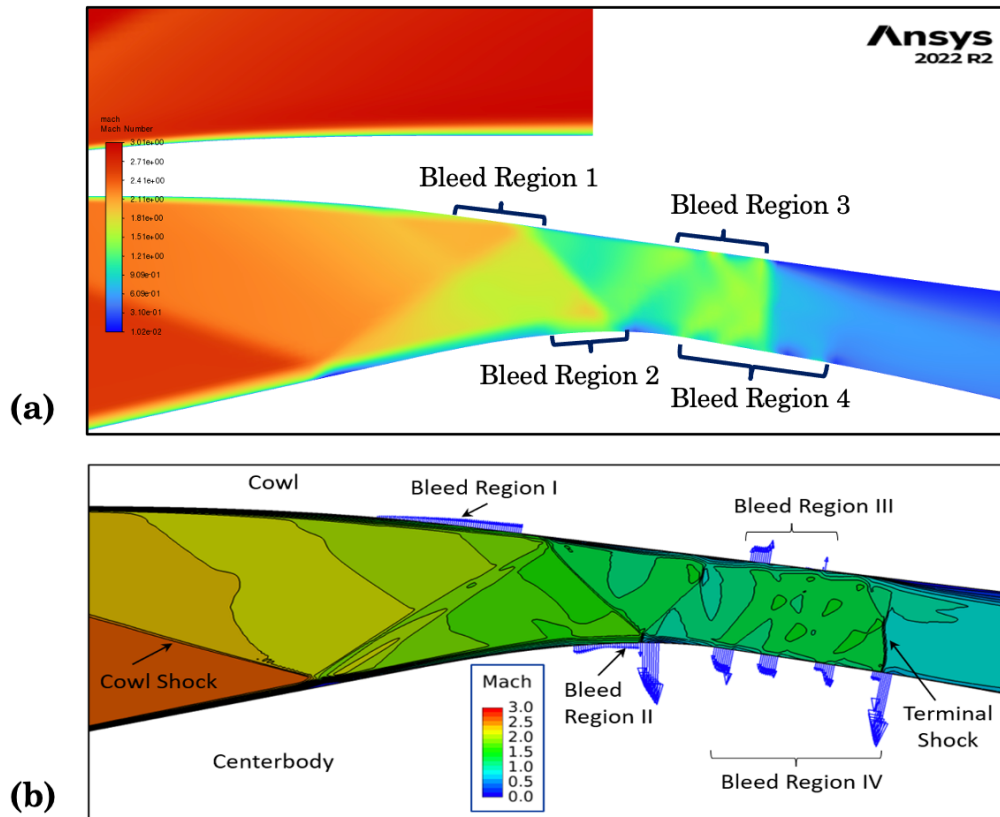


Figure 21: Comparison of Mach contours between (a) test case 2 and (b) PAW-6 published results [2].

Conclusion

This was a challenging problem aimed at analyzing flow through a supersonic inlet with resolving an internal shock structure, porous bleed zones, and shock-boundary layer interactions. The NASA 1507 inlet geometry was used to generate two unstructured meshes, a coarse grid of 42,885 cells and a medium grid of 92,753 cells with inflation layers near the walls. The difference in grid sizes helped to more closely evaluate the shock-boundary layer interactions and the bleed zones' impact. The back pressure was varied at the outlet and in the bleed zones which resulted in the terminal/normal shock to move closer to the throat with increasing backpressure. ANSYS Fluent was utilized using a two-stage solver approach. First Order Upwind method was first used until the residuals converged or began to oscillate around 10^{-3} . Then the solver was run using the Second Order Upwind method for the flow and the turbulent dissipation rates, and the QUICK method for the turbulent kinetic energy until the residuals either converged or oscillated around one point for around a thousand iterations. Using this approach helped to avoid unstart of the inlet. Initially there were issues with convergence, but after implementation of this method, the solution approached a converged or nearly converged state.

The results indicate that the inlet's internal shock structure turns the flow slowly through oblique shocks before terminating in a normal shock. This produces subsonic flow at the engine face, as required for normal engine operation, with minimal total pressure losses and reduced entropy. Shock-boundary layer interactions resulted in increased boundary layer thickness after an oblique shock. The bleed zones energize the boundary layer and reduce its size, thereby preventing boundary layer separation. To test off-design performance of the inlet for the extra assignment, the simulation was run at Mach 2 with the boundary conditions of test case 2. This

resulted in the formation of a detached bow shock at the front face of the inlet. Though subsonic flow was achieved at the engine face, the total pressure losses were significant. Further, our simulation results were compared to the simulation results provided in the PAW-6 handout. The internal shock pattern and shock-boundary layer interactions are nearly identical. The primary difference between the two sets of results is the location of the normal shock. In the published results, the normal shock is slightly downstream of the normal shock in our results.

References

- [1] Sorensen, N. E., and Smeltzer, D. B. *Investigation of an Axisymmetric Inlet System Capable of High-Performance at Mach Numbers 0.6 to 5.0*. NASA TM X-1507, February 1968.
- [2] AIAA Propulsion Aerodynamics Workshop. *NASA 1507 Inlet Briefing Pack*. 6th AIAA Propulsion Aerodynamics Workshop, January 21-22, 2023. National Harbor, MD, USA.